PERIODICUM BIOLOGORUM
VOL. 126, No 1–2, 63–74, 2024
DOI: 10.18054/pb.v126i1-2.30749

UDC 57:61
CODEN PDBIAD
ISSN 0031-5362

Original research article

MicroRNAs involved in the toxic effects of sodium arsenite on chicken skin fibroblasts

MEI JIN
HONGBO ZHANG
WEIYU FAN
HAIXU QIN
LEI ZHOU
FENGQIN ZHAO*

Liaoning Provincial Key Laboratory of Biotechnology and Drug Discovery, Liaoning Normal University, Dalian, China

***Correspondence:**
Fengqin Zhao
E-mail address: eco-env@163.com

Abbreviations

CSFs	– chicken skin fibroblasts
DEGs	– differentially expressed genes
DEmiRNAs	– differentially expressed microRNAs
ERS	– endoplasmic reticulum stress
GO	– Gene Ontology
IC_{50}	– semi-inhibitory concentrations
KEGG	– Kyoto Encyclopedia of Genes and Genomes
SA	– sodium arsenite

Keywords: sodium arsenite; fibroblasts; microRNA; apoptosis; transcriptome sequencing

Received April 22, 2024
Revised October 12, 2024
Accepted October 12, 2024

Abstract

Background and purpose: *Arsenic is a naturally occurring metalloid and environmental pollutant, which has shown its bidirectional regulatory effect on cell proliferation. Research on the toxic effects of sodium arsenite (SA) on chicken skin fibroblasts (CSFs) is limited. Research indicates that microRNAs and mRNAs can regulate apoptosis. Therefore, this study aimed to explore whether SA exerts toxic effects on CSFs through microRNAs and mRNAs.*

Materials and methods: *CSFs were treated with different concentrations (0-120 μmol/L) of SA for 12 h, 24 h, 48 h and 72 h, and the cell viability was detected by MTT assay. Transmission electron microscopy, flow cytometry, comet assay, and western blotting, were employed to detect cell morphology, apoptosis, DNA damage and protein levels, respectively, and the toxic effect of SA on CSFs was studied. Transcriptome sequencing and bioinformatics tools were used to analyze the expression and function of differentially expressed microRNAs (DEmiRNAs) and differentially expressed genes (DEGs).*

Results: *The proliferative, critical, and semi-inhibitory concentrations (IC_{50}) of SA on CSFs were 0.10, 0.25, and 16.35 μmol/L, respectively, within 24 hours. 16.35 μmol/L SA caused abnormal cell morphology, increased DNA damage, and induced apoptosis via the endoplasmic reticulum stress (ERS) and death receptor pathways. In this study, transcriptome sequencing and bioinformatics analysis suggested that 16.35 μmol/L SA might promote CSFs apoptosis through the microRNA-mRNA network.*

Conclusions: *At a concentration of 0.10 μmol/L, SA promoted cell proliferation. Concentrations exceeding 0.25 μmol/L inhibited cell proliferation and induced apoptosis through the ERS and death receptor pathways. MicroRNAs played a role in the toxic effects of SA on CSFs by interacting with target genes.*

INTRODUCTION

Arsenic (As), a metalloid element found in nature, exists in both inorganic and organic forms within ecosystems. The most prevalent and toxic form of arsenic in the environment is inorganic trivalent arsenite *(1)*. Generally, low doses of arsenic are beneficial to organisms and are widely used to promote animal growth *(2)*. However, high doses of arsenic are detrimental. Kao *et al.* found that low doses of arsenic stimulated cell proliferation and induced cancer in bladder epithelial cells, while high doses exhibited toxicity by triggering cell death *(3)*. Hoang *et al.* studied leukemic stem cells and demonstrated that arsenic trioxide

induced apoptosis by upregulating ROS-induced stress on DNA repair mechanisms *(4)*. Yamaguchi *et al.*, using mouse skin fibroblasts, found that 10 ppm arsenate hindered cell proliferation and disrupted the cell cycle *(5)*. Additionally, arsenic accumulates in the skin by binding to thiol-rich epidermal keratin *(6)*. As a result, the skin is one of the most sensitive organs to As exposure and is often the first site of arsenic poisoning symptoms. Arsenic can also enter the bodies of chickens through skin contact, food ingestion, and other routes, accumulating in target organs like the skin and leading to skin lesions. However, the toxic effects of As on chicken skin have not been thoroughly studied. Inorganic arsenic is easier than organic arsenic to enter living organisms and bind to sulfhydryl groups (-SH), making it easy to accumulate in skin, hair, and other parts *(7–10)*. Trivalent inorganic arsenic is the most toxic and usually exists in the form of arsenite, with sodium arsenite (SA) being a common arsenite. SA can induce oxidative damage, inflammation and apoptosis, and has toxic effects on cells *(11–13)*. Therefore, it is essential to further investigate the dose-effect relationship of sodium arsenite (SA) on chicken skin cytotoxicity and to explore the mechanisms underlying its toxic effects.

In recent years, in animal husbandry, arsenic-containing feed additives have been used to promote the growth of livestock and poultry and to prevent diseases. Drinking water also contains significant amounts of arsenic, which can be ingested by chickens through food and water, accumulating in the skin and other commonly used tissues. This accumulation has a series of effects on the skin, a target organ of arsenic, leading to skin lesions in chickens. Skin fibroblasts are the predominant type of mesenchymal cells in connective tissue, and studies have shown that fibroblasts have the ability to "reprogram" the skin and play a key role in skin wound healing and repair *(18)*. Therefore, the toxic effects of SA on the morphological structure, DNA damage and apoptosis of chicken skin fibroblasts (CSFs) were studied.

MicroRNAs (miRNAs) are small RNA molecules, approximately 20-25 nucleotides in length *(19)*. They regulate gene expression by altering the targeted mRNA's stability and/or translation efficiency *(20)*. miRNAs are crucial for various cellular processes and are known to affect significant biological processes, including apoptosis *(21)*. Arsenic can regulate the expression of miRNAs in cells, thereby influencing cell growth. For example, Zhang observed that arsenic sulfide impeded the invasion and migration of gastric cancer cells through the induction of miR-4665-3p *(22)*. In another study, S Zhang *et al.* found that arsenic trioxide suppressed the growth and migration of breast cancer cells by downregulating miR-27a *(23)*. Additionally, Zhang *et al.* reported that arsenic trioxide induced apoptosis in retinoblastoma cells by modulating the expression of miR-376a *(24)*. These studies demonstrate that arsenic can influence miRNA expression profiles in various cells, and miRNAs play a crucial regulatory role in arsenic-induced apoptosis. However, it remains unclear whether the miRNA expression profile is altered during SA-induced apoptosis in CSFs and whether miRNAs are involved in regulating this apoptosis process.

In conclusion, studies on the microRNA-mRNA network of SA regulating the morphological structure, DNA damage, and apoptosis of chicken skin fibroblasts (CSFs) are scarce. Therefore, we aim to analyze the effects of SA on the morphological structure, DNA damage, and apoptosis of CSFs by constructing a microRNA-mRNA regulatory network.

MATERIALS AND METHODS

Recovery and culture of CSFs: The CSFs samples were procured from Shanghai Saibaikang Co., Ltd. These were chest skin samples from chickens (Gallus gallus domesticus). Samples were cultured in iCell primary fibroblast medium (ICell Bioscience Inc, China), with FBS (Hyclone, USA), in a 37°C, 5% CO2 incubator.

MTT assay

Cell proliferation was detected by MTT assay *(25)*. The CSFs density in logarithmic growth phase was adjusted to 3×104 cells/mL and inoculated in 96-well cell culture plates with 100 µL per well and 3 replicate wells per concentration gradient. Sodium arsenite (Sigma, USA) was diluted with complete medium and cells were treated with different concentrations (0-120 µmol/L) of SA. The cells were incubated in 37°C, 5% CO_2 for 12 h, 24 h, 48 h, and 72 h. 10 µL of MTT (Sigma, USA) was added to the wells for 4 h of incubation in the dark. Cell culture medium was removed, they were then dissolved in 200 µL DMSO, shaken for 10 min, and the absorbance value at 492 nm was detected (Thermo MK3, USA). The measured absorbance values were used to analyse the effects of cell proliferation and inhibition.

TEM preparation

Cells were collected after 24 h of treatment with 0, 0.10, 0.25 and 16.35 µmol/L SA, fixed with fixatives for observation with electron microscopy, and they were post-fixed with 1% osmic acid. Samples were sequentially dehydrated in graded ethanol (50%, 70%, 80%, 90%, 95%, 100%, 100%) and 100% acetone, each step lasting 15 min. Protocol 1:1 acetone with embedding medium 812 and incubate for 2-4 hours. Protocol additional acetone and embedding medium 812 in a 2:1 ratio and infiltrate overnight. Samples were then embedded in pure embedding medium 812 for 5-8 hours, set in embedding plates, and processed at 37°C. After 48 h polymerization at 60°C, samples were sectioned ultrathin, stained with ura-

nyl acetate and lead citrate solution for 15 min, and then dried for electron microscopy (JEOL, Japan).

Detection of apoptosis by flow cytometry: After treating the cells with 0, 0.10, 0.25 and 16.35 µmol/L SA for 24 h, cells were digested with trypsin without EDTA, then washed with 1*PBS (4°C), and mixed with 500 µL of 1× Binding Buffer. 5 µL of Annexin V-FITC (Kkey Biotech, China) was added and incubated for 15 min at room temperature in the dark. Following this, 5 µL PI (propidium iodide) was added for staining and incubated for 10 min at room temperature, also in the dark. Cells were then resuspended in PBS and analyzed by flow cytometry (BD, USA), with the excitation wavelength (Ex) and the emission wavelength (Em) of 488 nm and 530 nm, respectively.

Comet assay

DNA damage was detected by the comet assay *(26)*. Cells were collected after 24 h of treatment with 0, 0.10, 0.25 and 16.35 µmol/L SA. 150 µL of 1% normal melting point agarose (NMA) (preheated at 56°C) was dropped onto the slide, immediately covered, and then kept at 4°C for 10 min. 10 µL of PBS (containing 1000 cells) and 100 µL of 0.8% low melting point agarose (LMA) were added onto the slides at 37°C to form the second and third gel layers. After 1 h of cell lysis at 4°C, the slides were washed twice with PBS and alkylated for 20 min at room temperature. Electrophoresis was conducted at room temperature, 1 V per centimeter, and 300 mA for 20 min. The slides were then neutralized with Tris-HCl (pH 7.5) for 15 min and stained with 50 µL of 30 µg/mL ethidium bromide (EB) solution in the dark for 20 min and observed by fluorescence microscope. The analysis was performed using CASP comet analysis software (Beijing Baile Liangcheng Technology Co., Ltd., China), with 50 cells per sample counted, using the comet tail DNA content (TDNA%) as a descriptor.

Fluo-3 AM fluorescent probe method

Fluo-3 AM fluorescent probe method was used to detect fluorescent calcium ions. Cells were harvested after 24 h of treatment with 0, 0.10, 0.25 and 16.35 µmol/L SA. An equal volume of 20% Pluronic F127 solution was mixed with the Fluo-3 AM/DMSO solution, then diluted with HBSS to make a 5 µM Fluo-3 AM working solution. This solution was added to the cells and incubated for 20 min at 37°C. Then, fluorescent calcium ion detection was performed with a fluorescence microscope (Mshot, China) with the excitation wavelength of 465-495 nm and the emission wavelength of 515-555 nm. The change in the concentration of calcium ions in the cell is reflected by the change in fluorescence intensity.

Quantitative Real-time PCR

Cells were collected after 24 h of treatment with 0, 0.10, 0.25 and 16.35 µmol/L SA. Total RNA was extracted using a total RNA extraction kit (Conway century, China) as per the manufacturer's instructions. The extracted RNA was reverse transcribed into cDNA using a reverse transcription kit (Beijing GMO Biological Technology Co., LTD, China). Primer sequences (Table 1) were sourced from Shanghai Shenggong Biosynthesis (Shanghai, China). Gene transcription levels were analyzed using the SYBRGreen PCR kit on a real-time PCR detector. GAPDH was employed as an internal reference gene. The relative expression of each target gene was analyzed using the $2^{-\Delta\Delta Ct}$ method.

Protein quantitative detection by Western Blot

Cells were harvested after 24 h of treatment with 0, 0.10, 0.25, and 16.35 µmol/L SA. Proteins were extracted using 400 µL of RIPA lysate (Biyuntian, China) containing 1 mM PMSF serine protease inhibitor. The protein samples were separated by sodium dodecyl sulphate-poly-

Table 1. *Primers used in qRT-PCR.*

Gene symbol	Forward primer (5'-3')	Reverse primer (5'-3')
GRP78	AGACTTTGACCAGCGTGTTATG	TCTACTTCCCGTCTTAGTTTCTGTA
IRE1α	TATCCAATGAGCGTACATCAGCA	CAGATCACTGGGAGCACGAAA
JNK	TGATCCATCAGAAGCCGAAGC	TGCCCACGTATAACCCCATT
PERK	ACTGGGCGAGGATGTTGTCT	TGAGTTCGGCGTAACAGGAGA
TNFR1	CCACCATCTGTTCCTCTGCTA	TGCTCCATCTCAATTCGCTCTA
FAS	ACTCTTCCACCTGCTCCTCATC	TTCGTGCAGCACTGACCACT
FADD	CAACTGATCGCAAGTTACAACG	GCTGGCTTCTCCCTCCTCTAT
Caspase10	ATGGCAGCGTTCAGAAGACC	CATTGCTTGGCAGTGAAGTAGG
Caspase3	AAGATGGACCACGCTCAG	TCTCGGTGGAAGTTCTTATTG
GAPDH	CAGAACATCATCCCAGCGTC	GGCAGGTCAGGTCAACAAC

acrylamide gel electrophoresis (SDS-PAGE) and transferred to a polyvinylidene difluoride (PVDF) membrane. The membrane was blocked in 5% non-fat dry milk for 2 h and then incubated overnight at 4°C with diluted primary antibodies: anti-GRP78 (HUABIO, HA722202, China; dilution 1:1000) and anti-GAPDH (wanleibio, WL01114, China; dilution 1:2000). Following this, the membrane was incubated with sheep anti-rabbit IgG-HRP secondary antibody (Abclonal, China) for 1 h. The ECL color development solution was then applied to the PVDF membrane, and the image was captured using a chemiluminescence imager (Tanon, China).

Total RNA extraction and transcriptome sequencing

Cells were collected after 24 h of treatment with 0 and 16.35 μmol/L SA. Total RNA was extracted using the Trizol reagent (Invitrogen, USA). The cDNA library was constructed from this RNA. The mRNAs were reverse transcribed into cDNA and synthesized into double-stranded DNA. This DNA was then PCR-amplified with specific primers(BGI, China), and the PCR product was heat-denatured to yield single-stranded DNA. The DNA was circularized with cross-linking primers to create a single-stranded circular DNA library, which was sequenced on the DNBSEQ-T7 platform with a PE150 read length. Transcriptome sequencing results were used to screen the differentially expressed genes (DEGs) of the SA IC_{50} group compared to the control group.

Screening of DEmiRNAs/DEGs

DEmiRNAs: Sequencing data was obtained and the DEseq2 method was employed to screen DEmiRNAs, with screening conditions set at $|\log_2 FC| \geq 1$ and Q value (padj.) ≤ 0.05. DEGs: Raw data underwent quality control (QC) to filter out low-quality reads containing connectors with unknown base N content greater than 5%. Clean reads were obtained and compared to a reference sequence using HISAT2. Gene expression levels were calculated using RSEM, and differential expression analysis was performed using DEseq.2. The screening condition for DEGs was $|\log_2 FC| \geq 1$ and Q value (Adjusted P value) ≤ 0.05.

GO/KEGG pathway functional enrichment analysis of DEmiRNAs and DEGs

Gene Ontology (GO) enrichment analysis: Candidate genes were matched to entries in the Gene Ontology database. The number of genes in each entry was counted, and a hypergeometric test was applied to identify candidate genes significantly enriched in relation to all background genes of a species. The P value was calculated using R's hypergeometric distribution function: phyper (https://stat.ethz.ch/R-manual/R-devel/library/stats/html/Hypergeometric.html). P values were then corrected, and multiple checks performed, using the Q value correction package. GO elements with a Q value (corrected p-value) ≤ 0.05 were considered significantly enriched among candidate genes.

Kyoto Encyclopedia of Genes and Genomes (KEGG) enrichment analysis

This analysis mirrored the GO functional enrichment analysis method. A final Q value ≤ 0.05 was considered indicative of significant enrichment of differentially expressed genes.

Construction of DEmiRNAs-DEGs network map

A combined analysis of DEmiRNAs and DEGs was conducted to identify hub genes. The intersection of miRNAs(down)-genes(up) and miRNAs(up)-genes(down) was predicted using HIPLOT PRO. The DEmiRNAs-DEGs network map was constructed using Cytoscape (version v3.9.1).

Statistical analysis

GraphPad Prism 9.5 software was utilized for statistical analysis. Data are presented as mean ± standard deviation. An unpaired t-test was used, with $P < 0.05$ considered significant and $P < 0.01$ considered extremely significant. Enrichment analysis was conducted using the Phyper feature of R software. The obtained P value was corrected by FDR to obtain the Q value, and a Q value ≤ 0.05 was deemed significantly enriched.

RESULTS

Effect of SA on the biological function of CSFs

At four time points, SA promoted cell proliferation at low concentrations and inhibited cell proliferation at higher concentrations (Figure 1A). The IC_{50} value at 24 h (16.35 μmol/L) was higher than at 48 h (6.99 μmol/L), with notable variation in concentration ranges. Subsequently, the control group (0 μmol/L), proliferation group (0.1 μmol/L), critical group (0.25 μmol/L), and IC_{50} group (16.35 μmol/L) under 24 h conditions were selected for further experiments. TEM observations showed that the morphological structure of cells in the control and proliferating groups was intact and clear (Figure 1B: c, d); the critical group displayed mild abnormalities, with a few mitochondria exhibiting solidified and expanded cristae (Figure 1B: e, f); the IC_{50} group cells exhibited severe abnormalities in morphology and structure, with more pronounced intracellular vacuoles, and the nucleus, chromatin, mitochondria, and endoplasmic reticulum appeared apoptotic (Figure 1B: g, h).

Flow cytometry results indicated that, compared with the control group, the percentage of apoptotic cells in the

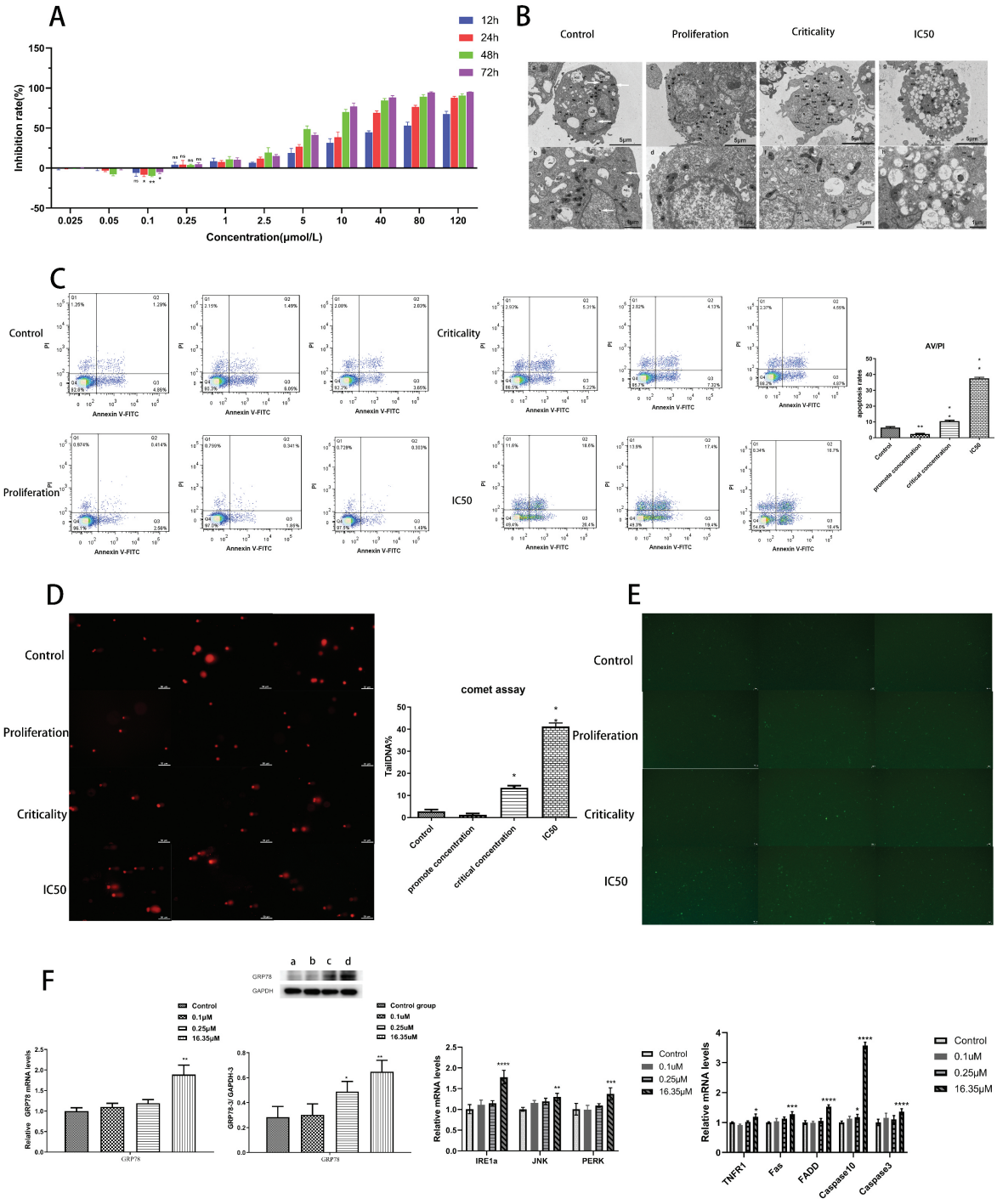

Figure 1. *Effect of SA on the biological function of CSFs. A: Cell proliferation was detected by MTT; B: Changes in organelles observed by TEM (The arrows point to the cell nucleus (N), mitochondria (M), and rough endoplasmic reticulum (RER). The scales are 5μm and 1μm); C: CSFs apoptosis was detected by flow cytometry (annexin V−/PI−: living cells; annexin V+/PI−: early apoptotic cells; annexin V+/PI+: late apoptotic cells; annexin V−/PI+: necrotic cells); D: DNA damage detected by comet assay (Scale: 50 μm); E: Calcium ion concentration detected by Fluo-3 AM fluorescent probe; F: The mRNA expression and protein levels were measured by qRT-PCR and western blot(a: Control, b: Proliferation, c: Criticality d: IC_{50}).*

proliferation group significantly decreased ($P < 0.01$), while in the critical and IC_{50} groups, it significantly increased ($P < 0.01$) (Figure 1C). Comet assay findings showed no trailing and no DNA damage in both control and proliferating cells, classifying them as grade 0 damage; the critical group exhibited slight trailing and mild DNA damage, classified as grade 1 damage; the IC_{50} group cells displayed pronounced comet-like trailing and

Table 2. *The level of DNA damage in CSFs treated with SA for 24 h.*

Group	Treatment time	DNA tail (%)	Degree of DNA damage (grade)
Control	24 h	2.86±2.40	0
Promote	24 h	1.24±1.86	0
Critical	24 h	13.51±2.76**	1
IC_{50}	24 h	41.31±4.68**	3

**Compared with the control group, P<0.01.

the most severe DNA damage, classified as grade 3 damage (Figure 1D, Table 2). These results suggest that high doses of SA can cause substantial DNA strand damage in CSFs.

The results of the Fluo-3 AM fluorescence probe for the detection of fluorescent calcium ions showed: the proliferation group had no significant change in fluorescence signal compared to the control group; the critical group exhibited slightly brighter fluorescence intensity and a higher amount of fluorescence; the IC_{50} group displayed the brightest fluorescence intensity and the highest number of fluorescence (Figure 1E). The qRT-PCR and Western Blot results showed that the mRNA expression and protein levels of GRP78, a marker of endoplasmic reticulum stress (ERS), did not change significantly in the promoter and critical groups compared to the control group (Figure 1F). However, these were highly upregulated in the IC_{50} group ($P < 0.001$). The expression of ERS apoptosis-related genes IRE1α, JNK, and PERK was also highly upregulated in the IC_{50} group (Figure 1F). This indicates that SA concentrations above 0.25 μmol/L can induce ERS and regulate apoptosis in CSFs by mediating

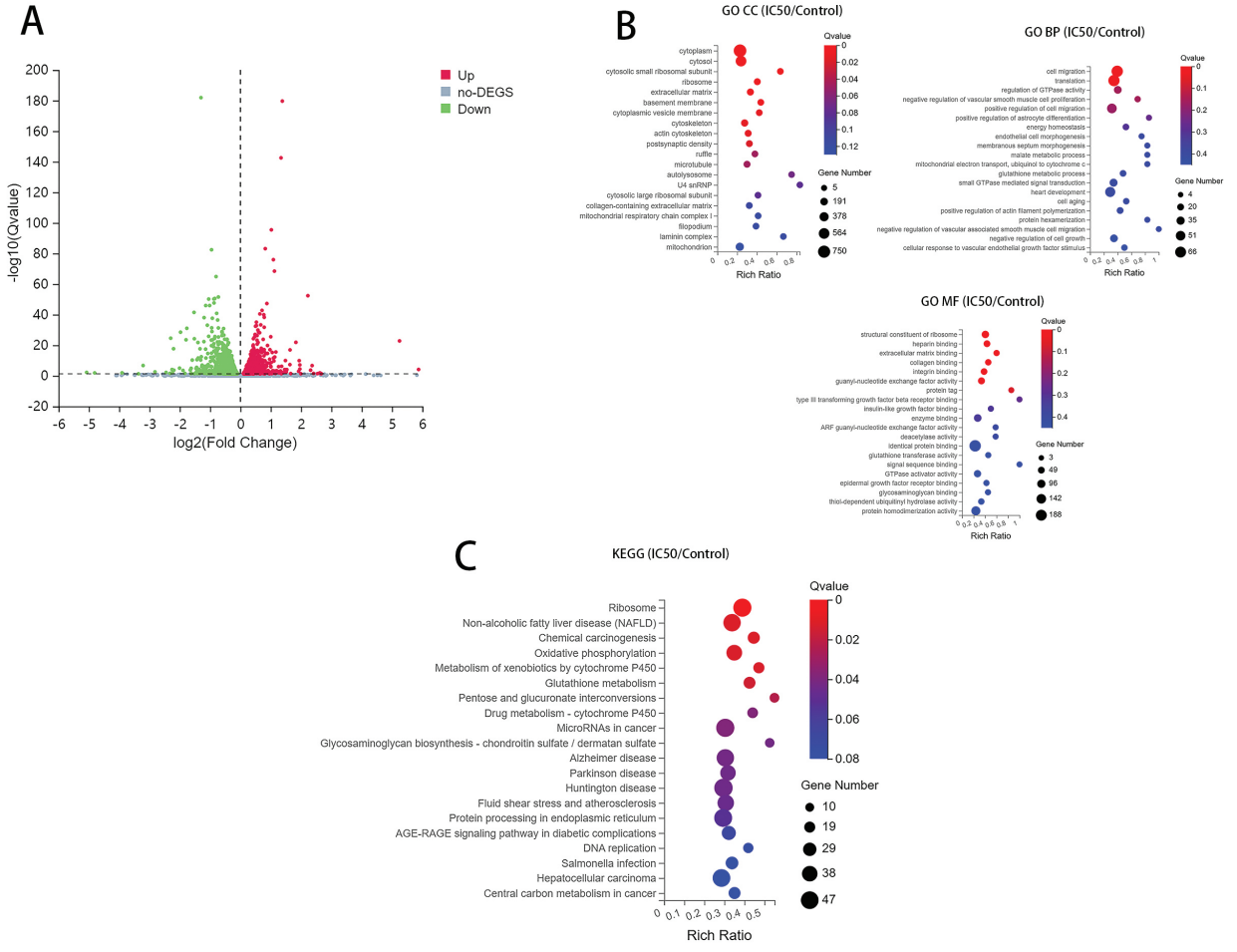

Figure 2. *Effect of SA on mRNA expression pattern in CSFs. A: Volcano plot of DEGs in IC_{50} group vs. control group; B: GO enrichment analysis of the DEGs; C: KEGG enrichment analysis of DEGs.*

ERS apoptosis-related genes. The qRT-PCR results also showed that the expression of death receptor pathway apoptosis-related genes TNFR1, FAS, FADD, Caspase10, and Caspase3 was significantly upregulated in the IC_{50} group compared with the control group (Figure 1F). This suggests that SA can also regulate apoptosis in CSFs by mediating death receptor pathway apoptosis-related genes.

Effect of SA on mRNA expression pattern in CSFs

Relative to the control group, the IC_{50} group exhibited a total of 2766 DEGs, with 1415 genes upregulated and 1351 genes downregulated (Figure 2A). GO enrichment analysis of these DEGs indicated primary functions in the cytoplasm, predominantly in biological processes such as transcriptional regulation of DNA template, positive regulation of transcription by RNA polymerase II, negative regulation of transcription by RNA polymerase II, and molecular functions including DNA binding, DNA-binding transcription factor activity, and DNA binding (Figure 2B). KEGG analysis revealed significant enrichment of the DEGs in the IC_{50} group across 14 signaling pathways, including ribosomal, chemical carcinogenesis, NAFLD, cytochrome P450 metabolism of xenobiotics, oxidative phosphorylation, glutathione metabolism, and the interconversion of pentose and glucuronide. Pathways with a high number of DEGs included ribosomes, NAFLD, and oxidative phosphorylation (Figure 2C).

Effect of SA on microRNA expression pattern in CSFs

Small RNA sequencing analysis in the CSFs post SA treatment in the IC_{50} group identified 16 DEmiRNAs, with an equal number (eight each) of upregulated and

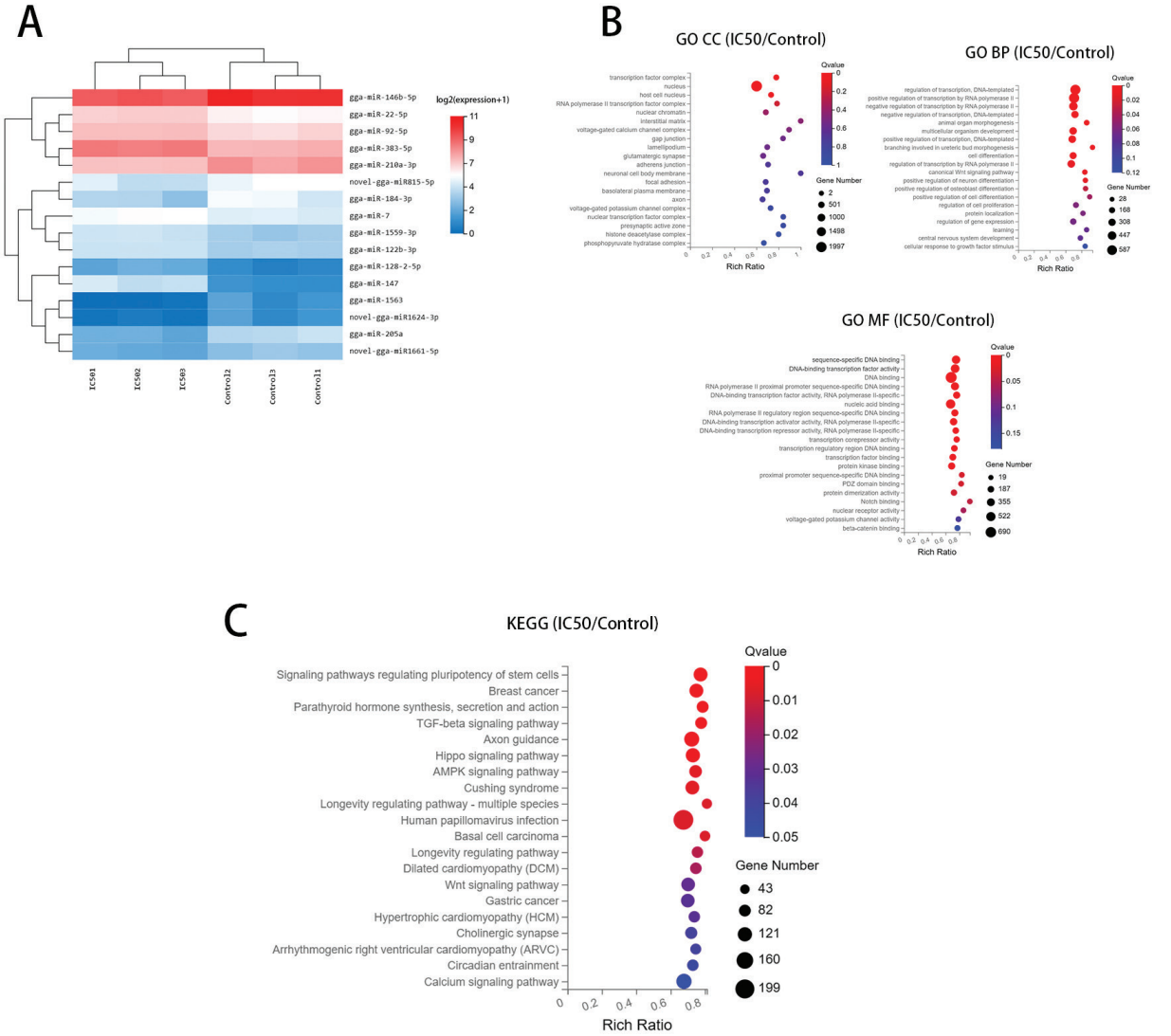

Figure 3. *Effect of SA on microRNA expression pattern in CSFs. A: Cluster heat-map analysis of the DEmiRNAs(the horizontal axis is the log² (expression value + 1) of the sample, and the vertical axis is the DEmiRNAs, the redder the color, the higher the expression, the bluer the color, the lower the expression); B: GO enrichment analysis of DEmiRNAs target genes; C: KEGG enrichment analysis of DEmiRNAs target genes.*

downregulated miRNAs. Among these, 13 were known miRNAs (gga-miR-122b-3p, gga-miR-128-2-5p, gga-miR-147, gga-miR-1559-3p, gga-miR-22-5p, gga-miR-383-5p, gga-miR-7, gga-miR-92-5p, gga-miR-146b-5p, gga-miR-1563, gga-miR-184-3p, gga-miR-205a, gga-miR-210a-3p), and 3 were newly discovered (novel-gga-miR1624-3p, novel-gga-miR1661-5p, novel-gga-miR815-5p). Clustering analysis of DEmiRNAs indicated distinct expression patterns in cells from the IC_{50} and control groups, with each group forming its own cluster (Figure 3A). GO enrichment analysis of the predicted target genes showed that target genes of DEmiRNAs were enriched in the categories of biological processes, cellular components, and molecular functions. In biological processes, significant enrichment was observed in transcriptional regulation DNA template, RNA polymerase II positive transcriptional regulators, and RNA polymerase II negative transcriptional regulators; in cellular components, enrichment was found in transcription factor complex, cell nucleus, and host cell nucleus; in molecular functions, the enrichment was in sequence-specific DNA binding, DNA-binding transcription factor activity, and DNA binding. These findings suggest that the enriched target genes are closely associated with transcriptional functions (Figure 3B). KEGG enrichment analysis of the predicted target genes of DEmiRNAs were significantly enriched across 20 pathways, including those regulating stem cell pluripotency, parathyroid hormone synthesis, secretion, and action, TGF-β, axon guidance, Hippo, AMPK, longevity regulatory pathway-multispecies, Wnt. Notably, the TGF-β, Hippo, Wnt, and calcium signaling pathways, associated with apoptosis, suggest that miRNAs can regulate apoptosis through interactions with target genes in the presence of SA (Figure 3C).

Construction of microRNA-mRNA regulatory networks by co-analysis

In analyzing the interaction between miRNAs and target genes, we observed an overlap of 594 genes between the target genes of down-regulated miRNAs and up-regulated genes (Figure 4A), and an overlap of 486 genes

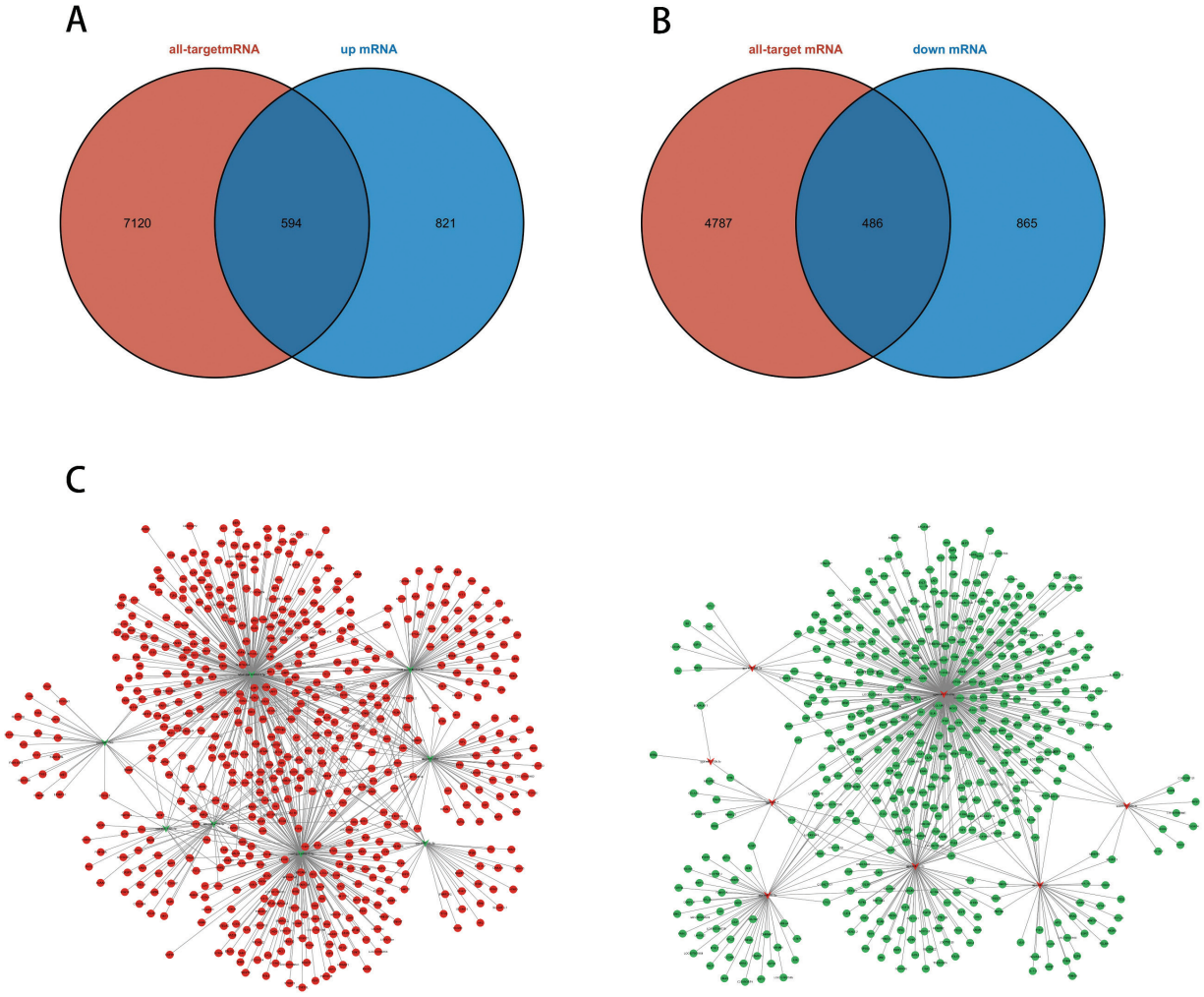

Figure 4. *The microRNA-mRNA regulatory network. A: The overlap of miRNAs(down)-genes(up); B: The overlap of miRNAs(up)-genes(down); C: DEmiRNAs-DEgene network map (V-shaped for miRNAs, round for genes; red for upregulated expression, green for downregulated expression).*

between the target genes of up-regulated miRNAs and down-regulated genes (Figure 4B). These findings enabled the construction of miRNAs(down)-genes(up) and miRNAs(up)-genes(down) target regulation networks, grounded in the negative regulatory relationships between miRNAs and their target genes. In the CSFs post SA treatment, differentially expressed miRNAs constituted a comprehensive regulatory network, comprising 782 miRNAs(down)-genes(up) regulatory axes involving 8 down-regulated miRNAs and 594 up-regulated genes, and 581 miRNAs(up)-genes(down) regulatory axes involving 8 up-regulated miRNAs and 486 down-regulated genes. This suggests that SA may selectively target these miRNAs-genes for cellular regulation (Figure 4C).

DISCUSSION

In this study, MTT assays were used to assess the proliferation and inhibition of CSFs exposed to different concentrations of SA for 12, 24, 48, and 72 h. The results showed that SA exerted bidirectional regulation in CSFs, and the effect was most obvious at 24 h. The specific results showed that SA concentration was 0.00-0.25 μmol/L, which could induce the proliferation of CSFs, and the best promotional effect was at 0.10 μmol/L. Concentrations above 0.25 μmol/L resulted in toxic effects, with a IC_{50} of 16.35 μmol/L.

In order to further illustrate the toxic effect of SA on CSFs, TEM was implemented in this study to observe the changes in CSFs after SA poisoning. According to TEM observations, low doses of SA did not induce cellular edema, but high SA doses did. Specifically, cellular edema marked cellular damage. Moreover, CSFs treated with a high SA dose demonstrated a marked increase in heterochromatin, which may deactivate transcriptional functions. These cells also showed degranulated RER and a lower number of ribosomes, suggesting inhibition of protein production and significant toxicity on the internal structure of CSFs. These observations were consistent with the MTT results, indicating that SA at concentrations above 0.25 μmol/L would have a cytotoxic effect on CSFs, affect cell proliferation, destroy the internal structure of cells, and cause damage to CSFs.

Additionally, flow cytometry was employed to assess apoptosis in each group following SA treatment. The results indicated that after 24 h, 0.10 μmol/L SA significantly reduced the apoptosis rate in CSFs, while concentrations above 0.25 μmol/L significantly increased the apoptosis rate, indicating an apoptosis-promoting effect. However, different species exhibit varying susceptibility to arsenic and different responses to arsenic toxicity *(27–29)*. This variation may be attributed to differences in arsenic absorption capacity, which can result in varying levels of arsenic accumulation in cells and, consequently, different degrees of toxic effects.

When arsenic compounds enter living organisms, they attack DNA strands, causing breaks. Arsenic also readily binds to sulfhydryl groups, affecting protease activity, interfering with DNA synthesis and repair, and ultimately leading to DNA damage *(30, 31)*. In this study, cells in the control and proliferation groups showed no DNA damage. However, as the SA concentration increased, the DNA strands in cells exhibited significant damage, with a cell damage rate of 41.31±4.68 ($P<0.01$). These findings suggest that high doses of SA can induce DNA damage in CSFs. This is consistent with the findings of Yamanaka et al., who demonstrated that arsenic compounds could cause DNA strand breaks in cells *(32)*.

To determine whether SA-induced apoptosis of CSFs involves the ERS pathway, we measured changes in intracellular calcium concentration, as well as GRP78 mRNA and protein expression levels, in each group following SA treatment. The results showed that high concentrations of SA significantly increased intracellular calcium levels and elevated GRP78 mRNA and protein expression. These findings indicate that SA concentrations above 0.25 μmol/L trigger ERS. In severe cases, ERS can lead to apoptosis. This study also demonstrated that the expression of ERS-related apoptosis genes, including IRE1α, JNK, and PERK, was upregulated after treatment with SA at concentrations above 0.25 μmol/L, suggesting that ERS contributes to the increased apoptosis rate in CSFs caused by SA.

To explore whether SA-induced apoptosis in CSFs involves the death receptor pathway, we examined the expression of apoptosis-related genes in each group following SA treatment. The results revealed that the expression of death receptor pathway-related genes, including TNFR1, FAS, FADD, and Caspase3, was upregulated, with Caspase10 expression significantly increased after treatment with 0.25 μmol/L SA. After treatment with 16.35 μmol/L SA, the genes FAS, FADD, Caspase10, Caspase3, and TNFR1 were all significantly upregulated. These findings suggest that the increase in apoptosis rate in CSFs induced by SA is associated with the death receptor pathway. SA appears to mediate the death receptor pathway by promoting the expression of related genes, thereby increasing apoptosis. This is consistent with the findings of Zhao *et al.*, who reported that the death receptor pathway contributes to excessive apoptosis in the immune organs of chickens with subchronic arsenic poisoning *(33)*.

MicroRNAs (miRNAs) play a crucial role in regulating various biological processes, including development, cell proliferation, differentiation, and apoptosis, by regulating the expression of their target genes through post-transcriptional regulation *(34)*. Previous studies have shown that miRNAs are involved in the regulation of arsenic-induced apoptosis, leading us to hypothesize that miRNAs may be one of the mechanisms through which SA induces apoptosis in CSFs. In this study, we identified

2,766 DEGs such as CNN2, PSMD4, and CSF1, and 16 DEmiRNAs, including miR-146b-5p, miR-147, miR-184-3p, miR-383-5p, miR-7, miR-22-5p, and miR-205a in the IC_{50} group compared to the control group through sequencing. Some of the DEGs and DEmiRNAs identified were closely associated with apoptosis *(35–40)*. These findings suggest that SA can alter the expression of miRNAs and mRNAs in CSFs, and it is speculated that DEmiRNAs may contribute to SA-induced apoptosis in CSFs by interacting with target genes.

Gene Ontology (GO) enrichment analysis of the DEmiRNAs and DEGs revealed that DEGs were highly enriched in cellular processes, metabolic processes, and catalytic activities. KEGG enrichment analysis showed that DEGs were significantly enriched in pathways related to ribosome function, oxidative phosphorylation, and glutathione metabolism, all of which are closely linked to the toxic effects of SA. The target genes of the DEmiRNAs were most significantly enriched in GO categories such as transcriptional regulation by RNA polymerase II, transcription factor complexes, nucleus, sequence-specific DNA binding, and DNA-binding transcription factor activity. These findings suggest that SA may induce apoptosis by disrupting DNA transcription in CSFs, leading to DNA damage. Furthermore, KEGG pathway enrichment analysis of the DEmiRNAs revealed that their target genes were significantly enriched in the TGF-β, Hippo, Wnt, and calcium signaling pathways, all of which are closely related to apoptosis *(41–43)*. These results indicate that SA may engage intracellular signaling pathways through the microRNA-mRNA network, resulting in abnormal cell morphology, DNA damage, and the promotion of apoptosis.

CONCLUSIONS

This paper focused on the toxic effects of SA on the morphological structure, DNA damage, and apoptosis of CSFs through a microRNA-mRNA network. Our findings indicate that SA at a concentration of 0.1 μmol/L enhanced cell proliferation. However, concentrations exceeding 0.25 μmol/L inhibited cell proliferation, and at 16.35 μmol/L, SA caused significant internal cellular damage, inducing apoptosis, DNA damage, and endoplasmic reticulum stress. By utilizing sequencing technology and qRT-PCR experiments, we analyzed the functional classification and signaling pathways of Sanhuang chicken skin cells' response to arsenic toxicity post SA treatment. The construction of a microRNA-mRNA regulatory network for SA in regulating the morphological structure, DNA damage, and apoptosis of CSFs provides a fundamental theoretical framework for further investigating the toxic effects of arsenic on chicken skin cells.

Acknowledgment: *We would like to thank R&S Biotechnology Company (Shanghai, China) very much for the hard work in performing lentiviral vectors targeting noggin and KAP26.1. We would also like to thank National Natural Science Foundation of China (No. 31172188), Agricultural Science and Technology Innovation Program of China (No. ASTIP-IAS13) very much for supporting this study. This research has been supported within the content of National Natural Science Foundation of China [grant number 31772557]; Dalian Science and Technology Innovation Fund Project [grant number 2019J12SN65].*

REFERENCES

1. TAM L M, JIANG J, WANG P, WANG Y 2020 Arsenite Binds to ZNF598 to Perturb Ribosome-Associated Protein Quality Control. Chem Res Toxicol 33: 1644-1652. https://doi.org/10.1021/acs.chemrestox.9b00412
2. ZHANG Y, WANG Y, LU Q, XIN W, CUI W, ZHU J 2016 Organoarsenic Roxarsone Promotes Angiogenesis In Vivo. Basic Clin Pharmacol Toxicol 118: 259-270. https://doi.org/10.1111/bcpt.12501
3. KAO Y T, WU C H, WU S Y, LAN S H, LIU H S, TSENG Y S 2017 Arsenic treatment increase Aurora-A overexpression through E2F1 activation in bladder cells. BMC Cancer 17: 277. https://doi.org/10.1186/s12885-017-3253-1
4. HOANG D H, BUETTNER R, VALERIO M, GHODA L, ZHANG B, KUO Y H, ROSEN S T, BURNETT J, MARCUCCI G, PULLARKAT V, NGUYEN L X T 2022 Arsenic Trioxide and Venetoclax Synergize against AML Progenitors by ROS Induction and Inhibition of Nrf2 Activation. Int J Mol Sci 23: 1-14. https://doi.org/10.3390/ijms23126568
5. YAMAGUCHI Y, MADHYASTHA H, MADHYASTHA R, CHOIJOOKHUU N, HISHIKAWA Y, PENGJAM Y, NAKAJIMA Y, MARUYAMA M 2016 Arsenic acid inhibits proliferation of skin fibroblasts, and increases cellular senescence through ROS mediated MST1-FOXO signaling pathway. J Toxicol Sci 41: 105-113. https://doi.org/10.2131/jts.41.105
6. XU B, WANG Y 2020 Indurated Papules and Skin Discolouration in a Patient: A Quiz. Acta Derm Venereol 100: adv00279. https://doi.org/10.2340/00015555-3646
7. ZHAO R, HOU Y, XUE P, WOODS C G, FU J, FENG B, GUAN D, SUN G, CHAN J Y, WAALKES M P, ANDERSEN M E, PI J 2011 Long isoforms of NRF1 contribute to arsenic-induced antioxidant response in human keratinocytes. Environ Health Perspect 119: 56-62. https://doi.org/10.1289/ehp.1002304
8. ROY N K, MURPHY A, COSTA M 2020 Arsenic Methyltransferase and Methylation of Inorganic Arsenic. Biomolecules 10: 1-13. https://doi.org/10.3390/biom10091351
9. ŁOŹNA K, STYCZYŃSKA M, BRONKOWSKA M, FIGURSKA-CIURA D, BIERNAT J 2014 Arsenic contents in rats' fur as an indicator of exposure to arsenic. Preliminary studies. Rocz Panstw Zakl Hig 65: 287-290.
10. KHAIRUL I, WANG Q Q, JIANG Y H, WANG C, NARANMANDURA H 2017 Metabolism, toxicity and anticancer activities of arsenic compounds. Oncotarget 8: 23905-23926. https://doi.org/10.18632/oncotarget.14733
11. AKBARI S, AMIRI F T, NADERI M, SHAKI F, SEYEDABADI M 2022 Sodium arsenite accelerates D-galactose-induced aging in the testis of the rat: Evidence for mitochondrial oxidative damage, NF-kB, JNK, and apoptosis pathways. Toxicology 470: 153148. https://doi.org/10.1016/j.tox.2022.153148
12. SUNTARARUKS S, WORASUTTAYANGKURN L, AKANIMANEE J, SURIYO T, NOOKABKAEW S, SRISAMUT N, VISITNONTHACHAI D, WATCHARASIT P, SATAYAVIVAD J 2019 Sodium arsenite exposure impairs B cell proliferation and enhances vascular inflammation in Plasmodium ber-

ghei mouse model. Environ Toxicol Pharmacol 66: 7-13. https://doi.org/10.1016/j.etap.2018.12.010

13. IVANOV V N, WEN G, HEI T K 2013 Sodium arsenite exposure inhibits AKT and Stat3 activation, suppresses self-renewal and induces apoptotic death of embryonic stem cells. Apoptosis 18: 188-200. https://doi.org/10.1007/s10495-012-0779-1
14. NYALALA I, OKINDA C, KUNJIE C, KOROHOU T, NYALALA L, CHAO Q 2021 Weight and volume estimation of poultry and products based on computer vision systems: a review. Poult Sci 100: 101072. https://doi.org/10.1016/j.psj.2021.101072
15. JI G G, ZHANG M, LIU Y F, SHAN Y J, TU Y J, JU X J, ZOU J M, SHU J T, WU J F, XIE J F 2021 A gene co-expression network analysis of the candidate genes and molecular pathways associated with feather follicle traits of chicken skin. J Anim Breed Genet 138: 122-134. https://doi.org/10.1111/jbg.12481
16. SEO M K, NA K W, HAN S H, PARK S H, HA S D 2020 Inhibitory effect of ethanol and thiamine dilaurylsulfate against loosely, intermediately, and tightly attached mesophilic aerobic bacteria, coliforms, and Salmonella Typhimurium in chicken skin. Poult Sci 99: 1571-1580. https://doi.org/10.1016/j.psj.2019.10.058
17. NISHIMURA S, ARAI S, OHTANI M, SHIMOMURA Y, TABATA S 2022 Effects of Estradiol on Expression of Estrogen Receptor and Collagen mRNAs in Chick Skin. J Poult Sci 59: 162-167. https://doi.org/10.2141/jpsa.0210093
18. THANGAPAZHAM R L, DARLING T N, MEYERLE J 2014 Alteration of skin properties with autologous dermal fibroblasts. Int J Mol Sci 15: 8407-8427. https://doi.org/10.3390/ijms15058407
19. MA R, WANG C, WANG J, WANG D, XU J 2016 miRNA-mRNA Interaction Network in Non-small Cell Lung Cancer. Interdiscip Sci 8: 209-219. https://doi.org/10.1007/s12539-015-0117-8
20. AFONSO-GRUNZ F, MüLLER S 2015 Principles of miRNA-mRNA interactions: beyond sequence complementarity. Cell Mol Life Sci 72: 3127-3141. https://doi.org/10.1007/s00018-015-1922-2
21. CHEN L, HEIKKINEN L, WANG C, YANG Y, SUN H, WONG G 2019 Trends in the development of miRNA bioinformatics tools. Brief Bioinform 20: 1836-1852. https://doi.org/10.1093/bib/bby054
22. ZHANG X, TAN Z, KANG T, ZHU C, CHEN S 2019 Arsenic sulfide induces miR-4665-3p to inhibit gastric cancer cell invasion and migration. Drug Des Devel Ther 13: 3037-3049. https://doi.org/10.2147/DDDT.S209219
23. ZHANG S, MA C, PANG H, ZENG F, CHENG L, FANG B, MA J, SHI Y, HONG H, CHEN J, WANG Z, XIA J 2016 Arsenic trioxide suppresses cell growth and migration via inhibition of miR-27a in breast cancer cells. Biochem Biophys Res Commun 469: 55-61. https://doi.org/10.1016/j.bbrc.2015.11.071
24. ZHANG Y, WU J H, HAN F, HUANG J M, SHI S Y, GU R D, CHEN X L, HE B 2013 Arsenic trioxide induced apoptosis in retinoblastoma cells by abnormal expression of microRNA-376a. Neoplasma 60: 247-253. https://doi.org/10.4149/neo_2013_033
25. DING J, LU X 2018 Expression of miR-204 in pediatric retinoblastoma and its effects on proliferation and apoptosis of cancer cells. Oncol Lett 16: 7152-7157. https://doi.org/10.3892/ol.2018.9519
26. COLLINS A, MøLLER P, GAJSKI G, VODENKOVá S, ABDULWAHED A, ANDERSON D, BANKOGLU E E, BONASSI S, BOUTET-ROBINET E, BRUNBORG G, CHAO C, COOKE M S, COSTA C, COSTA S, DHAWAN A, DE LAPUENTE J, BO C D, DUBUS J, DUSINSKA M, DUTHIE S J, YAMANI N E, ENGELWARD B, GAIVãO I, GIOVANNELLI L, GODSCHALK R, GUILHERME S, GUTZKOW K B, HABAS K, HERNáNDEZ A, HERRERO O, ISIDORI M, JHA A N, KNASMüLLER S, KOOTER I M, KOPPEN G, KRUSZEWSKI M, LADEIRA C, LAFFON B, LARRAMENDY M, HéGARAT L L, LEWIES A, LEWINSKA A, LIWSZYC G E, DE CERAIN A L, MANJANATHA M, MARCOS R, MILIĆ M, DE ANDRADE V M, MORETTI M, MURUZABAL D, NOVAK M, OLIVEIRA R, OLSEN A K, OWITI N, PACHECO M, PANDEY A K, PFUHLER S, POURRUT B, REISINGER K, ROJAS E, RUNDéN-PRAN E, SANZ-SERRANO J, SHAPOSHNIKOV S, SIPINEN V, SMEETS K, STOPPER H, TEIXEIRA J P, VALDIGLESIAS V, VALVERDE M, VAN ACKER F, VAN SCHOOTEN F J, VASQUEZ M, WENTZEL J F, WNUK M, WOUTERS A, ŽEGURA B, ZIKMUND T, LANGIE S A S, AZQUETA A 2023 Measuring DNA modifications with the comet assay: a compendium of protocols. Nat Protoc 18: 929-989. https://doi.org/10.1038/s41596-022-00754-y
27. WANG Y C, CHAUNG R H, TUNG L C 2004 Comparison of the cytotoxicity induced by different exposure to sodium arsenite in two fish cell lines. Aquat Toxicol 69: 67-79. https://doi.org/10.1016/j.aquatox.2004.04.007
28. ANWAR N, QURESHI I Z, SPEARS N, LOPES F 2020 In vitro administration of sodium arsenite in mouse prepubertal testis induces germ cell loss and apoptosis. Toxicol In Vitro 67: 104924. https://doi.org/10.1016/j.tiv.2020.104924
29. VEGA L, MONTES DE OCA P, SAAVEDRA R, OSTROSKY-WEGMAN P 2004 Helper T cell subpopulations from women are more susceptible to the toxic effect of sodium arsenite in vitro. Toxicology 199: 121-128. https://doi.org/10.1016/j.tox.2004.02.012
30. WANG T S, HSU T Y, CHUNG C H, WANG A S, BAU D T, JAN K Y 2001 Arsenite induces oxidative DNA adducts and DNA-protein cross-links in mammalian cells. Free Radic Biol Med 31: 321-330. https://doi.org/10.1016/S0891-5849(01)00581-0
31. RAMANATHAN K, SHILA S, KUMARAN S, PANNEERSELVAM C 2003 Ascorbic acid and alpha-tocopherol as potent modulators on arsenic induced toxicity in mitochondria. J Nutr Biochem 14: 416-420. https://doi.org/10.1016/S0955-2863(03)00076-7
32. YAMANAKA K, TAKABAYASHI F, MIZOI M, AN Y, HASEGAWA A, OKADA S 2001 Oral exposure of dimethylarsinic acid, a main metabolite of inorganic arsenics, in mice leads to an increase in 8-Oxo-2'-deoxyguanosine level, specifically in the target organs for arsenic carcinogenesis. Biochem Biophys Res Commun 287: 66-70. https://doi.org/10.1006/bbrc.2001.5551
33. ZHAO H, HE Y, LI S, SUN X, WANG Y, SHAO Y, HOU Z, XING M 2017 Subchronic arsenism-induced oxidative stress and inflammation contribute to apoptosis through mitochondrial and death receptor dependent pathways in chicken immune organs. Oncotarget 8: 40327-40344. https://doi.org/10.18632/oncotarget.16960
34. YONG-HAO Y, XIAN-GUO W, MING X, JIN-PING Z 2019 Expression and clinical significance of miR-139-5p in non-small cell lung cancer. J Int Med Res 47: 867-874. https://doi.org/10.1177/0300060518815379
35. HU J, XIE W, SHANG L, YANG X, LI Q, XU M, DOU J, ZHOU Y, NIU W, WU Y 2017 Knockdown of calponin 2 suppressed cell growth in gastric cancer cells. Tumour Biol 39: 1010428317706455. https://doi.org/10.1177/1010428317706455
36. LI Y, ZHOU Q, SHEN J, ZHU L 2021 Down-regulation of PSMD4 can attenuate autophagy, enhance the accumulation of intracellular ROS, and increase the sensitivity of epithelial ovarian cancer to carboplatin by inhibiting the NF-κB pathway. Transl Cancer Res 10: 4756-4772. https://doi.org/10.21037/tcr-21-1389
37. LIAO W, HE X J, ZHANG W, CHEN Y L, YANG J, XIANG W, DING Y 2022 MiR-145 participates in the development of lupus nephritis by targeting CSF1 to regulate the JAK/STAT signaling pathway. Cytokine 154: 155877. https://doi.org/10.1016/j.cyto.2022.155877

38. ZHANG L H, JIANG S Z, GUO X, XIAO B, LI Q, CHEN J Y, HUANG J R, RAO H 2021 MiR-146b-5p targets IFI35 to inhibit inflammatory response and apoptosis via JAK1/STAT1 signalling in lipopolysaccharide-induced glomerular cells. Autoimmunity 54: 430-438. https://doi.org/10.1080/08916934.2020.1864730

39. DU Y, YANG F, LV D, ZHANG Q, YUAN X 2019 MiR-147 inhibits cyclic mechanical stretch-induced apoptosis in L6 myoblasts via ameliorating endoplasmic reticulum stress by targeting BRMS1. Cell Stress Chaperones 24: 1151-1161. https://doi.org/10.1007/s12192-019-01037-4

40. GRIECO G E, BRUSCO N, FIGNANI D, NIGI L, FORMICHI C, LICATA G, MARSELLI L, MARCHETTI P, SALVINI L, TINTI L, PO A, FERRETTI E, SEBASTIANI G, DOTTA F 2022 Reduced miR-184-3p expression protects pancreatic β-cells from lipotoxic and proinflammatory apoptosis in type 2 diabetes via CRTC1 upregulation. Cell Death Discov 8: 340. https://doi.org/10.1038/s41420-022-01142-x

41. ZHAO H W, LI Y W, FENG R, YU J B, LI J, ZHANG Y, LI J C, WANG Y X 2015 TGF-β/Smad2/3 signal pathway involves in U251 cell proliferation and apoptosis. Gene 562: 76-82. https://doi.org/10.1016/j.gene.2015.02.049

42. MENG F, XIE B, MARTIN J F 2022 Targeting the Hippo pathway in heart repair. Cardiovasc Res 118: 2402-2414. https://doi.org/10.1093/cvr/cvab291

43. CHEN J, WANG X, ZHANG J, CHANG J, HAN C, XU Z, YU H 2022 Effects of the Wnt/β-Catenin Signaling Pathway on Proliferation and Apoptosis of Gastric Cancer Cells. Contrast Media Mol Imaging 2022: 5132691. https://doi.org/10.1155/2022/5132691